Supplementary Information for

Matrix Effects on the Performance and Mechanism of Hg Removal from Groundwater by MoS₂ Nanosheets

Mengxia Wang[a], Qi Han,[a] Yufei Shu,[a] Kunkun Wang,[a] Li Wang,[a]

Bei Liu,[a] Ines Zucker,[b] and Zhongying Wang[a*]

[a] State Environmental Protection Key Laboratory of Integrated Surface Water-Groundwater Pollution Control, Guangdong Provincial Key Laboratory of Soil and Groundwater Pollution Control, School of Environmental Science and Engineering Southern University of Science and Technology, Shenzhen 518055, China

[b] Porter School of Environmental Studies and School of Mechanical Engineering,

Tel Aviv University, 69978, Israel

---

[*] to whom correspondence should be addressed.   e-mail: wangzy6@sustech.edu.cn;   tel.: +86-075588018040;

Table of Contents

Materials

All chemicals used in this study were of analytical grade or higher. Sodium sulfate (Na$_2$SO$_4$) and sodium bicarbonate (NaHCO$_3$) were obtained from Linfeng Chemical Reagent Technology (Shanghai, China). Mercury nitrate (Hg(NO$_3$)$_2$·H$_2$O) was purchased from Macklin Chemical Reagent Technology (Shanghai, China). Calcium chloride anhydrous (CaCl$_2$) and sodium chloride (NaCl) were obtained from Guoyao Chemical Reagent Corporation (Shanghai, China).

Sorption kinetic and isotherm models

The commonly used pseudo-first-order (**Eq. (1)**) and pseudo-second-order (**Eq. (2)**) kinetic models were employed to evaluate the controlling of kinetic mechanism of adsorption process, and the relative model equations are presented in the following:[1]

$$In(q_e - q_t) = Inq_e - K_1t \tag{1}$$

$$\frac{t}{q_t} = \frac{1}{K_2 q_e^2} + \frac{t}{q_e} \tag{2}$$

where q_t and q_e (mg/g) represent the Hg uptake at time t (h) and equilibrium, respectively; K_1 and K_2 are pseudo-first-order and pseudo-second-order sorption rate constants, respectively.

The isotherm data was fitted with the classical Langmuir (**Eq. (3)**) model and Freundlich model (**Eq. (4)**):

$$q_e = \frac{q_m K_L C_e}{1 + K_L C_e} \tag{3}$$

$$q_e = K_F C_e^{\frac{1}{n}}$$

(4)

where q_e (mg/g) and C_e (mg/L) are the equilibrium Hg uptake and the equilibrium Hg

concentration, q_m (mg/g) is the monolayer maximum sorption capacity, and K_L (L/mg)

is the Langmuir affinity constant. K_F is the Freundlich affinity coefficient

[(mg/g)/(mg/L)^n], and n is the exponential coefficient.

Desorption tests

Before leaching tests, the Hg-laden MoS_2 and AC samples were prepared by adding 20

mg/L Hg(II) with either 8 mg/L MoS_2 nanosheets or 1.67 g/L activated carbon. The Hg

removal efficiency by MoS_2 nanosheets and AC were above 97%, indicating nearly

complete anchoring of Hg ions by MoS_2 and AC. Desorption tests were performed by

monitoring the Hg release from Hg-laden MoS_2 and AC samples in 20 mL simulated

groundwater, 20 mL acid solution (0.23 mM H_2SO_4 and 0.17 mM HNO_3), or 20 mL 1

mM EDTA solution. The mixture of solution of H_2SO_4 and HNO_3 was prepared at a

mass radio of 2:1 in DI water (pH = 3.2±0.1) to simulate the condition in which the

samples are exposed to acidic rain (HJ/T 299-2007, China).[2] In all cases, the vials were

sealed and continuously mixed on an end-over-end rotator at 60 rpm at room

temperature (25±1 ºC) for 1 d, 2 d, 4 d, and 7 d. The samples were filtered through the

0.22 μm PTFE filters and analyzed for Hg concentrations in the filtrates.

Table S1. Pseudo-first-order and pseudo-second-order models for simulating Hg sorption kinetics and the corresponding fitting parameters.

Kinetic models	Parameters			R^2
Pseudo-first-order	K_1 (h^{-1})	q_e (mg/g)	$h_1 = K_1 q_e$ (mg/(g•h))	0.9698
	0.97 ± 0.12	50.91 ± 1.18	49.38	
Pseudo-second-order	K_2 (g/(mg•h))	q_e (mg/g)	$h_2 = K_2 q_e^2$ (mg/(g•h))	0.9999
	0.075 ± 0.01	1250 ± 0.63	117187.5	

Table S2. Regression parameters of sorption isotherm data of Hg(II) onto MoS_2 nanosheets by Langmuir and Freundlich models.

Water bodies	Adsorption isotherm	Parameters		R^2
Groundwater	Langmuir	q_m (mg/g)	b (L/mg)	0.9801
		6288	1.82	
	Freundlich	K_F, (mg/g)/(mg/L)^n	n	0.9145
		3494.11	0.23	
DI Water	Langmuir	q_m (mg/g)	b (L/mg)	0.9592
		4042.85	0.41	
	Freundlich	K_F, (mg/g)/(mg/L)^n	n	0.9883
		1893.86	0.21	

Table S3. Comparison of the Hg removal capacities of different materials.

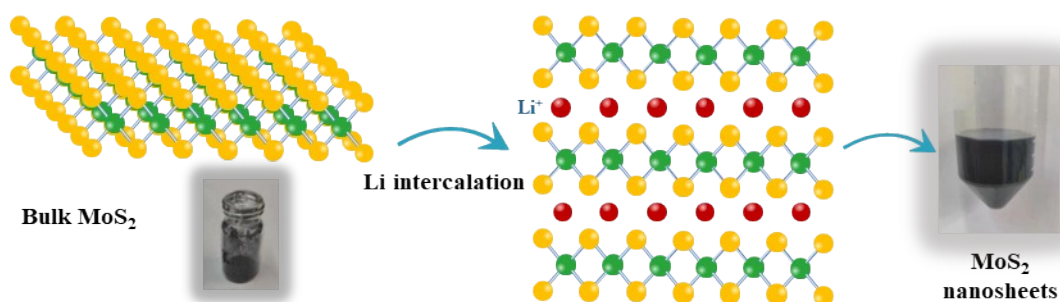| Adsorbent	Material Type	Capacity (mg/g)	Reference
Other Materials	FeS	3086.4	[3]
	Indium-modified ZVI	220.9	[4]
	Biochar	57.8	[5]
	SnS_2	185.83	[6]
	GO	255.1	[6]
	SGO/Fe-Mn	233.17	[7]
	Multilayered Ti_3C_2Ox Mxene	4806	[8]
MoS_2-based Materials	d-MoS_2/Fe_3O_4	425.5	[9]
	MoS_2-HNR	~1991	[10]
	Petal-like MoS_2	289	[11]
	□P-PVDF/MoS_2	578	[12]
	MoS_2/MMT	1836	[13]
	2D-MoS_2	6288	Our work

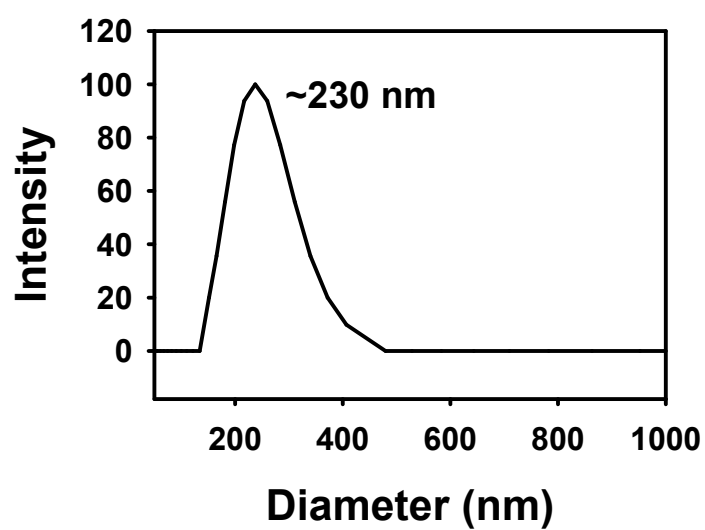**Figure S1**. Schematic illustration of the chemical exfoliation of bulk MoS$_2$.

Figure S2. Particle size distribution of as-exfoliated MoS$_2$ nanosheets measured by dynamic light scattering.
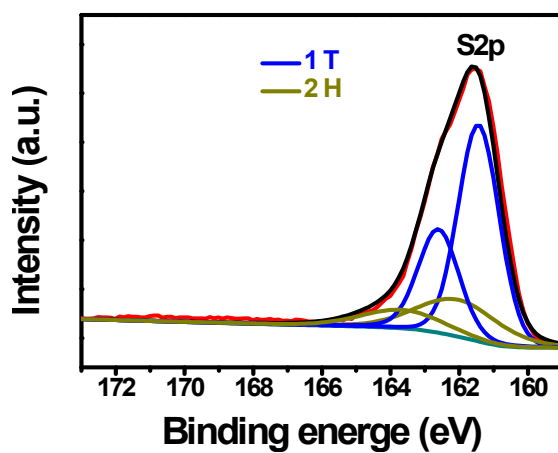

Figure S3. XPS S 2p spectra of as-prepared MoS$_2$ nanosheets.
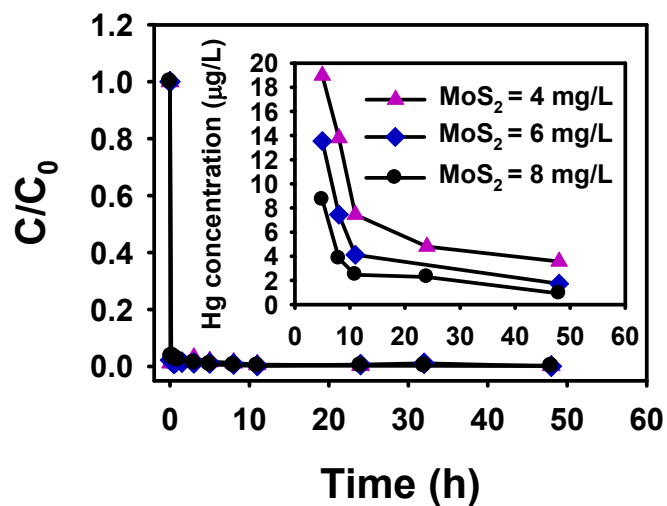
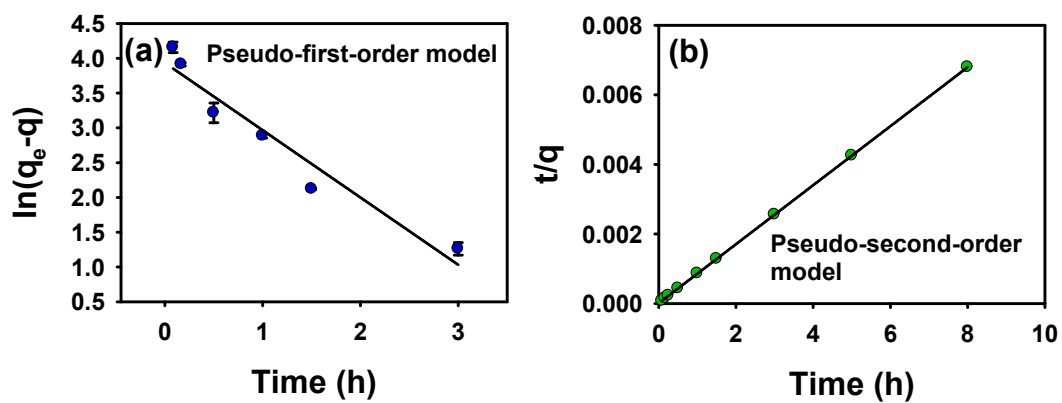**Figure S4**. Hg uptake kinetics by MoS_2 nanosheets in groundwater.

Figure S5. Hg uptake kinetics by MoS_2 nanosheets fitted with (a) pseudo-first-order model and (b) pseudo-second-order model.

Figure S6 content includes the table:

Table: Compared ICP and IC to determined The concentration of MoO_4^{2-} after Hg reacted with various MoS_2

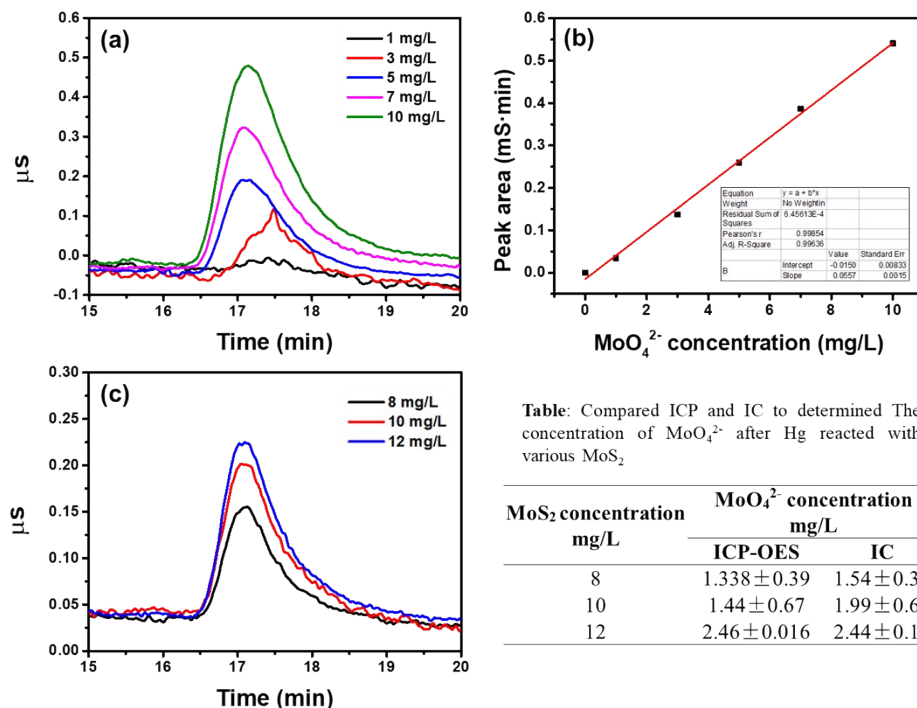| MoS_2 concentration mg/L	MoO_4^{2-} concentration mg/L	
	ICP-OES	**IC**
8	1.338 ± 0.39	1.54 ± 0.38
10	1.44 ± 0.67	1.99 ± 0.63
12	2.46 ± 0.016	2.44 ± 0.13

Figure S6. Determination of MoO_4^{2-} in solution by Ion Chromatography. (a) Chromatograms of different concentration of MoO_4^{2-} by the addition of sodium molybdate. (b) Linear relationship between MoO_4^{2-} concentration and peak area. (c) Ion Chromatograms of soluble Mo species after the reactions of Hg with MoS_2 at various concentrations. The concentrations of MoO_4^{2-} determined by ICP-OES and IC exhibited a good agreement (the inserted table).
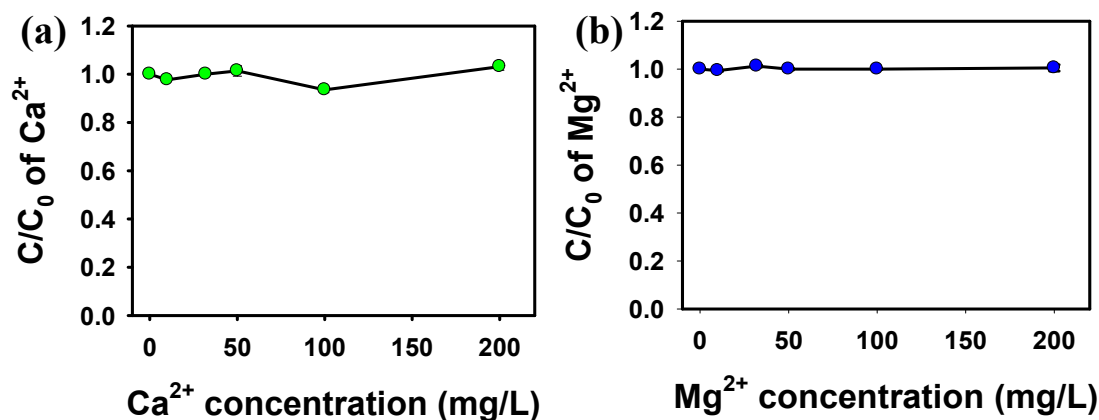

Figure S7. The ratios of the remaining to the initial concentrations of Ca^{2+} (a) and Mg^{2+} (b) in the presence of MoS_2 nanosheets.
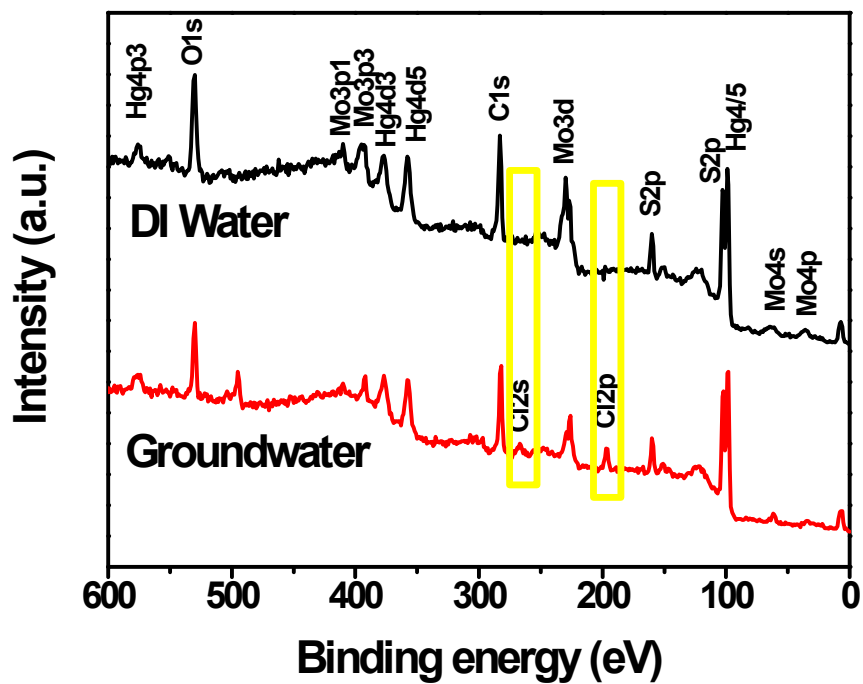
Figure S8. The XPS survey scan spectra of Hg-laden MoS_2 formed in DI water and Groundwater.
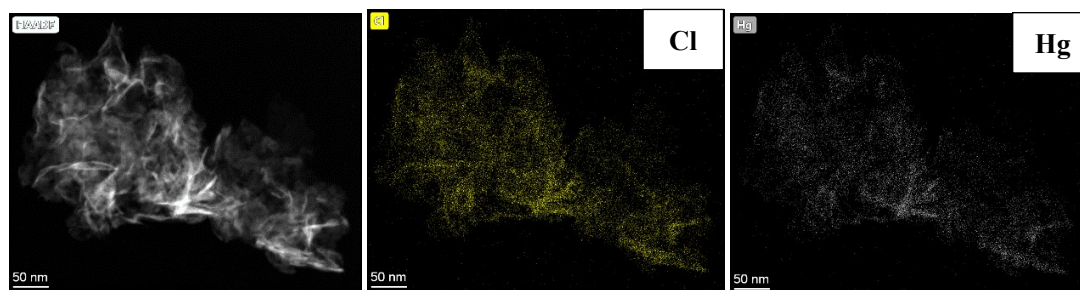

Figure S9. TEM images and EDS-mapping of Hg-laden MoS_2 nanosheets in groundwater.
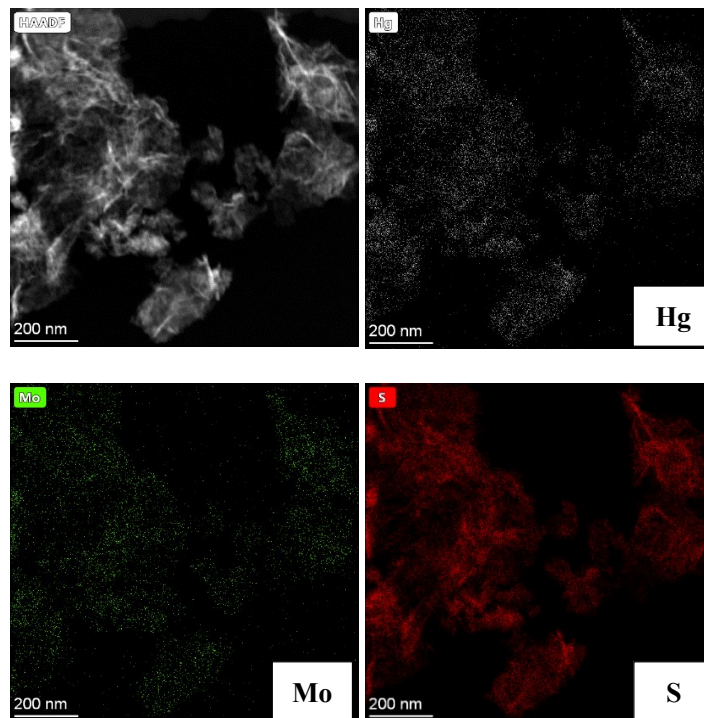
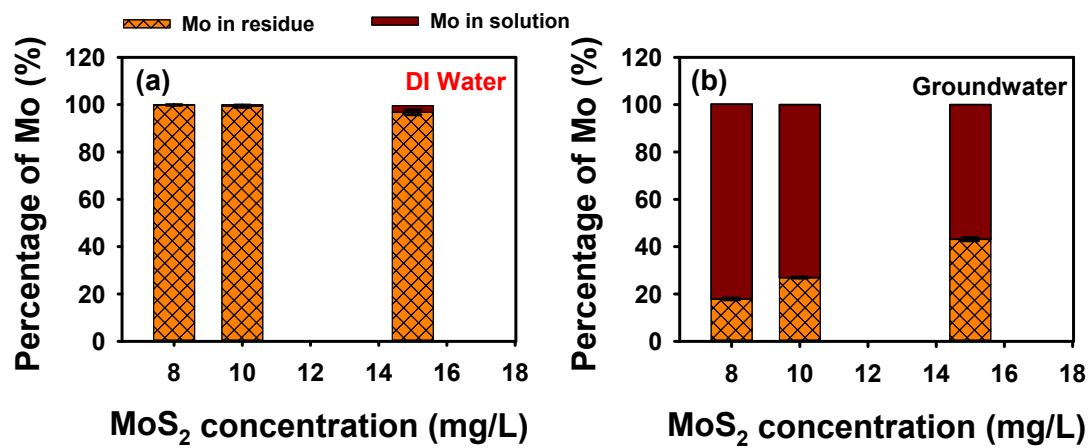**Figure S10**. TEM images and EDS-mapping of Hg-laden MoS$_2$ nanosheets in DI water.

Figure S11. Mass distributions of Mo species in (a) DI water and (b) groundwater.
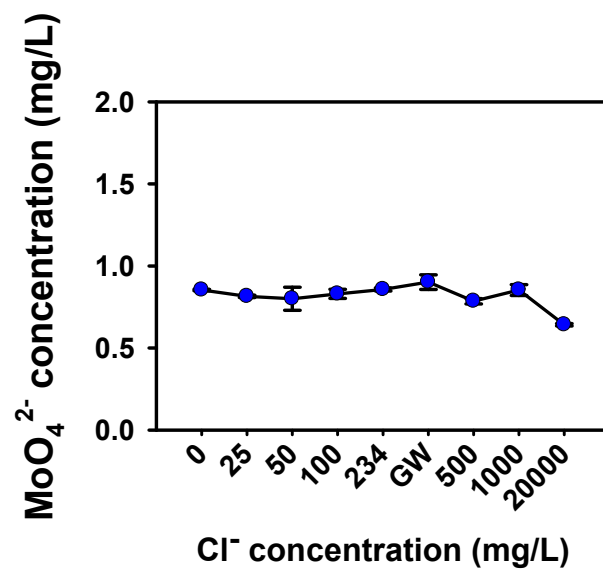
Figure S12. Oxidation of MoS$_2$ nanosheets in presence of Cl$^-$ at various concentrations.
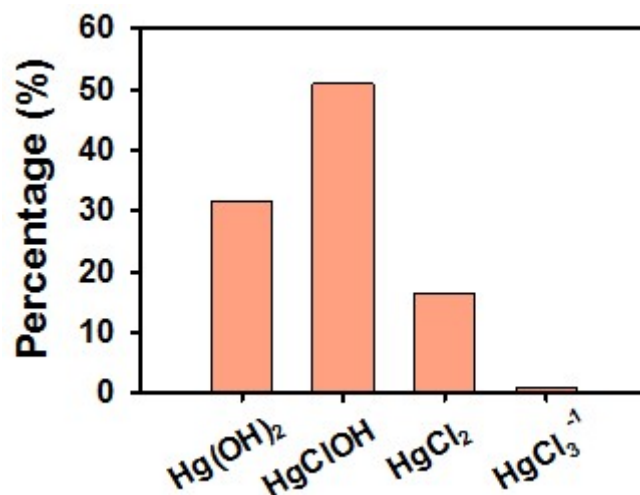

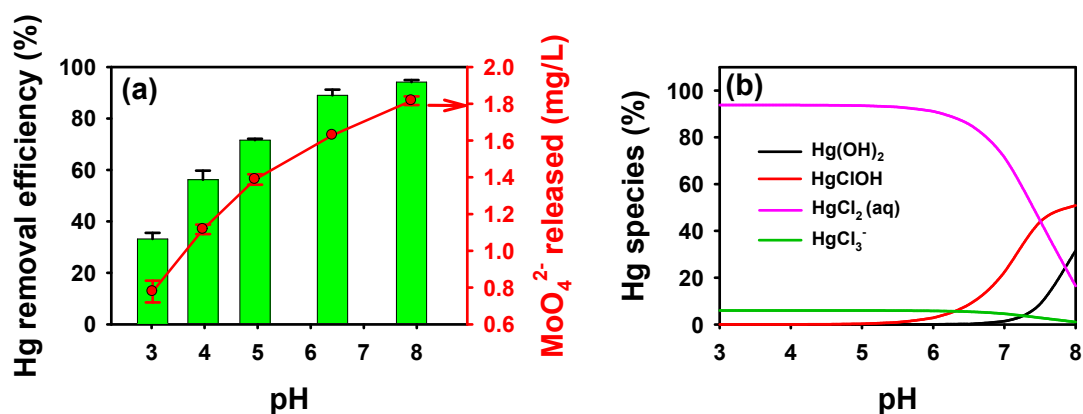**Figure S13**. The percentage of Hg species in simulated groundwater using Visual MINTEQ (version 3.1) at pH = 8.0.

Figure S14. (a) Effects of pH on Hg removal efficiency by MoS_2, Hg = 20 mg/L, MoS_2 = 4 mg/L. (b) Hg speciation as a function of pH determined by Visual MINTEQ.
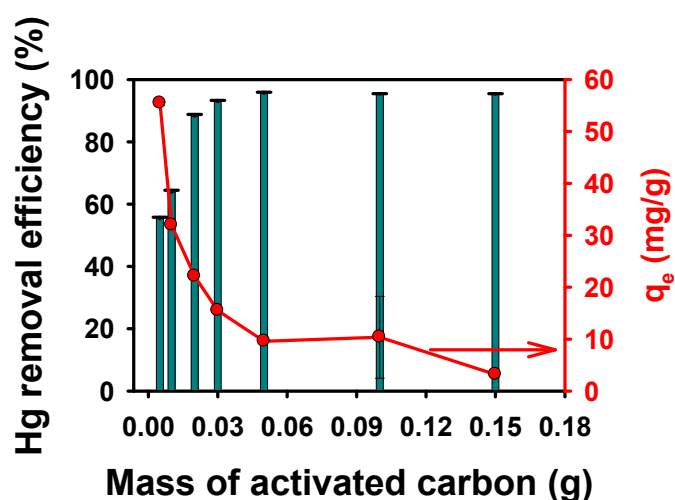

Figure S15. Hg uptake by AC in the groundwater. The mass of AC is 0–0.15 g, Hg concentration is 20 mg/L.

Reference

1   Y. Huang, S. Xia, J. Lyu and J. Tang, Highly efficient removal of aqueous Hg^{2+} and CH_3Hg^+ by selective modification of biochar with 3-mercaptopropyltrimethoxysilane, *Chem. Eng. J.*, 2019, **360**, 1646-1655.

2   Y. Huang, M. Wang, Z. Li, Y. Gong and E. Y. Zeng, In situ remediation of mercury-contaminated soil using thiol-functionalized graphene oxide/Fe-Mn composite, *J. Hazard. Mater.*, 2019, **373**, 783-790.

3   M. Wang, Y. Li, D. Zhao, L. Zhuang, G. Yang and Y. Gong, Immobilization of mercury by iron sulfide nanoparticles alters mercury speciation and microbial methylation in contaminated groundwater, *Chem. Eng. J.*, 2020, **381**, 122664.

4   G. H. Qasim, S. Lee, W. Lee and S. Han, Reduction and removal of aqueous Hg(II) using indium-modified zero-valent iron particles, *Appl. Catal B: Environ.*, 2020, **277**, 119198.

5   J. H. Park, J. J. Wang, B. Zhou, J. E. R. Mikhael and R. D. DeLaune, Removing mercury

from aqueous solution using sulfurized biochar and associated mechanisms, *Environ. Pollut.*, 2019, **244**, 627-635.

6   E. Rathore and K. Biswas, Selective and ppb level removal of Hg(II) from water: synergistic role of graphene oxide and SnS_2, *J. Mater. Chem. A.*, 2018, **6**, 13142-13152.

7   Y. Huang, Y. Gong, J. Tang and S. Xia, Effective removal of inorganic mercury and methylmercury from aqueous solution using novel thiol-functionalized graphene oxide/Fe-Mn composite, *J. Hazard. Mater.*, 2019, **366**, 130-139.

8   K. Fu, X. Liu, D. Yu, J. Luo, Z. Wang and J. C. Crittenden, Highly Efficient and Selective Hg(II) Removal from Water Using Multilayered $Ti_3C_2O_x$ MXene via Adsorption Coupled with Catalytic Reduction Mechanism, *Environ. Sci. Technol.*, 2020, **54**, 16212-16220.

9   Y. Song, M. Lu, B. Huang, D. Wang, G. Wang and L. Zhou, Decoration of defective MoS_2 nanosheets with Fe_3O_4 nanoparticles as superior magnetic adsorbent for highly selective and efficient mercury ions (Hg^{2+}) removal, *J. Alloys. Compds.*, 2018, **737**, 113-121.

10   A. N. Jayadharan Salini, A. Ramachandran, S. Sadasivakurup and S. K. Yesodha, Versatile MoS_2 hollow nanoroses for a quick-witted removal of Hg (II), Pb (II) and Ag (I) from water and the mechanism: Affinity or Electrochemistry?, *Appl. Mater. Today.*, 2020, **20**, 100642.

11   R. Pirarath, P. Shivashanmugam, A. Syed, A. M. Elgorban, S. Anandan and M. Ashokkumar, Mercury removal from aqueous solution using petal-like MoS_2 nanosheets, *Front. Environ. Sci. Eng.*, 2021, **15**.

12   X. Zhao, J. Li, S. Mu, W. He, D. Zhang, X. Wu, C. Wang and H. Zeng, Efficient removal of mercury ions with MoS_2-nanosheet-decorated PVDF composite adsorption membrane, *Environ. Pollut.*, 2021, **268**, 115705.

13   E. D. A. Mário, C. Liu, C. I. Ezugwu, S. Mao, F. Jia and S. Song, Molybdenum disulfide/montmorillonite composite as a highly efficient adsorbent for mercury removal from wastewater, *Appl Clay Sci.*, 2020, **184**, 105370.